JAAS

PAPER

View Article Online
View Journal

Cite this: DOI: 10.1039/c5ja00080g

Development of an isolation procedure and MC-ICP-MS measurement protocol for the study of stable isotope ratio variations of nickel†

Stepan M. Chernonozhkin,[a] Steven Goderis,[ab] Lara Lobo,[a] Philippe Claeys[ab] and Frank Vanhaecke*[a]

Received 10th March 2015
Accepted 22nd May 2015

DOI: 10.1039/c5ja00080g

www.rsc.org/jaas

Published on 22 May 2015. Downloaded by Universiteit Gent on 16/06/2015 13:15:23.

Variations in the isotopic composition of Ni resulting from natural mass-dependent processes in terrestrial or extraterrestrial conditions, inhomogeneous distribution of nucleosynthetic components and/or ingrowth from radioactive parent nuclides, help us to further understand the early formation history of Solar System materials and the nature of the processes these materials subsequently experienced. In studies of Ni isotope systematics, mass-dependent variations in the isotopic composition of Ni are often bypassed because of the challenges associated with the sample preparation. At the level of natural variation studied, Ni isotope ratio measurements are extremely sensitive to spectral interference, artificial on-column isotope fractionation and possibly even to the mass bias correction model applied. To adequately address these complications, an isolation procedure and measurement protocol relying on multi-collector ICP-mass spectrometry (MC-ICP-MS) have been designed and validated in this work. The overall reproducibility obtained based on repeated measurement of a Sigma-Aldrich high-purity Ni standard is 0.036‰, 0.049‰, 0.078‰ and 0.53‰ for $\delta^{60/58}$Ni, $\delta^{61/58}$Ni, $\delta^{62/58}$Ni and $\delta^{64/58}$Ni, respectively (n = 14; 2 SD). Nickel isotope ratio variations have been studied in a set of iron meteorites and geological reference materials, and the results obtained, except for those suffering from an elevated ^{64}Zn background, show good agreement with the available literature data. By using the flexible generalized power law with a variable discrimination exponent and the three-isotope method, the processes underlying natural mass fractionation of Ni for terrestrial reference materials were found to have a mixed equilibrium/kinetic nature. Mass-dependent Ni fractionation was observed between sample fractions of the Canyon Diablo iron meteorite, and the extracted fractionation factor β corresponds to isotope partitioning following the power law.

Introduction

In the process of the formation and evolution of meteorite parent bodies, the isotopic composition of various transition metals (*e.g.*, Fe, Cr, Ni, Cu, Zn) has been established to result from multiple superimposed processes, including nucleosynthesis in different stellar environments, (incomplete) mixing of the presolar carriers of these nucleosynthetic components in the crescent solar nebula, isotope fractionation during differentiation processes, ingrowth through radiogenic decay, and perturbation of the isotopic composition due to spallation by cosmic rays.[1,2]

In this context, isotopic analysis of Ni shows great potential for geo- and planetary applications. As an abundant element in the Solar System, Ni is present in sufficiently high concentrations in most meteorites. Ni, mostly partitioned into the metal–silicate–troilite system, experiences mass-dependent fractionation of its isotopes during evaporation/condensation, core formation, and magmatic processes. Other transition metals that have recently been studied in this context include Fe,[3] Cr,[4] Mo,[5] Zn[6] and W.[7] In contrast to other elements, Ni only occurs in a single stable oxidation state and surrounding coordination only, apart from its neutral metal state. Hence, redox-controlled mass-dependent fractionation processes do not affect the isotopic composition of Ni, restricting the mechanism underlying mass-dependent fractionation to isotopic exchange between phases.[8–11] A comparative study of the effect of mass-dependent isotope fractionation observed for Ni in genetically related meteorite fractions could not only show a correlation with the concentration of particular major elements (*e.g.*, P, S), but also with the cooling rate of the meteorite and/or the isotopic composition of other fractionated elements (*e.g.*, O, Cr).

[a]*Ghent University, Department of Analytical Chemistry, Krijgslaan, 281 – S12, 9000 Ghent, Belgium. E-mail: Frank.Vanhaecke@UGent.be*

[b]*Vrije Universiteit Brussel, Earth System Sciences, Pleinlaan 2, 1050 Brussels, Belgium*

† Electronic supplementary information (ESI) available. See DOI: 10.1039/c5ja00080g

Published on 22 May 2015. Downloaded by Universiteit Gent on 16/06/2015 13:15:23.

When applied to terrestrial igneous rocks, information on the mass-dependent isotope fractionation for Ni constitutes a useful marker of high-temperature processes and crystallization effects in magmatic systems.[9,11] Ni isotope fractionation processes appear to be systematic, with positive and negative fractionations, characteristic of low- and high-temperature processes, respectively.[8]

Ni isotope ratios were recently also used to track the process of continental weathering.[12,13] In addition, Ni isotope ratios can be used to highlight ancient ocean chemistry changes (*e.g.*, the decline of marine methanogens or the onset of the Great Oxidation Event)[14] *via* investigation of fractionation effects taking place during marine sedimentation,[15,16] in the water cycle,[17] or during interaction with biological systems.[13,18,19]

At the same time, mass-dependent fractionation of Ni isotopes occurring during the evolution of meteorite parent bodies can be quantified and cancelled out using mass-fractionation laws[20] and one pair of Ni isotopes that are not prone to non mass-dependent effects as internal standard. Different to some other elements (*e.g.*, W[21,22]), the neutron capture cross-sections are small for all Ni isotopes, making any resolvable cosmogenic spallation effects on Ni isotopes unlikely,[23,24] and thus, the pristine initial isotopic composition of Ni can be determined. As Ni has five isotopes, the remaining non mass-dependent effect on the Ni isotopic composition of extraterrestrial material (including pre-solar grains) – *i.e.* after removing the mass-dependent component – can refine our knowledge of the contributions of the different stellar nucleosynthetic sources to the solar nebula,[25] or permit insight into the homogeneity/heterogeneity of the distribution of Ni in the protosolar nebula to be obtained.[26] Information on the non mass-dependent effect on the Ni isotopic compositions can be used to evaluate possible mass-independent fractionation[23] (as Ni has both odd and even isotopes[27,28]) during the evolution of meteorite parent bodies. In addition, ^{60}Ni is a part of a short-lived isotopic decay system ($^{60}\mathrm{Fe} \rightarrow {}^{60}\mathrm{Ni} + \beta^- + \bar{\nu}$; $T_{1/2} = 2.62$ My)[29] that serves as a chronometer providing information on the time-scales of planetesimal melting and planetary differentiation, ultimately leading to core formation.[24] Because ^{60}Fe is produced in stars only, its initial abundance can be calculated to provide a constraint on the stellar contribution of radionuclides to the early Solar System and on the nature of this stellar source.[30]

Insight into the non mass-dependent contribution to the isotope fractionation observed for Ni in conjunction with other isotopic systems, such as those of O, Cr, Ti, can provide supporting evidence for petrogenic relationships between different meteorites and their groups.[4] As the non mass-dependent effect on the Ni isotopic compositions is interpreted to result from mixing of presolar sources, Ni isotope ratios provide knowledge on the genetic ancestry of particular meteorite groups.

MC-ICP-MS is a state-of-the-art analytical technique for isotopic analysis, but it requires target element isolation to reduce matrix effects and spectral interferences. At the same time, chromatographic isolation is known to introduce artificial isotope fractionation, which, together with the limited scale of Ni isotope ratio variations caused by natural fractionation, challenges Ni isotopic analysis. To avoid this undesirable bias during sample preparation, 100% recovery of Ni should be realized. After isolation, Ni mass-dependent isotope fractionation can be studied using MC-ICP-MS relying on an admixed internal standard (*e.g.*, Cu) for correction of instrumental mass discrimination or, alternatively, using the double-spike technique. The latter was often preferred in previous studies of Ni mass-dependent fractionation, as it is less sensitive to the isolation procedure. However, double-spiking is much more laborious and can typically provide information on a single Ni isotope ratio only.[8,31]

Although several studies of non mass-dependent isotope fractionation have focused on Ni, the robustness of the figures of merit achieved remains debatable. At the reported levels of precision, it remains unclear whether Ni isotope ratio data can be applied to study the problems discussed above, as the relevant levels of Ni fractionation are at the limit of the capabilities of the MC-ICP-MS technique (sub part per ten thousand units).

For the applications in which isotope ratios involving all of the Ni isotopes are required, clean lab conditions become crucial to produce reliable data for ratios involving ^{64}Ni. This is the least abundant Ni isotope, very sensitive to spectral interferences, especially as the result of isobaric overlap due to Zn contamination. As a result, adequate separation factors should be aimed at in the design of the isolation procedures. Also, the low isotopic abundance of ^{64}Ni (0.9255%)[32] deteriorates the precision of its measurement, and questions the utility of isotope ratios involving ^{64}Ni for the issues discussed above.

To overcome the challenges mentioned and understand which applications of Ni isotopic studies can be addressed by the current state-of-the-art analytical techniques, Ni isolation procedures, MC-ICP-MS measurement protocols and mass bias correction methods have to be evaluated and optimized.

Experimental

Reagents and samples

Only high-purity reagents and acids were used throughout the experiments. Pro analysis grade nitric acid (65%, Chem-Lab, Belgium) was further purified through sub-boiling in a PFA apparatus. Optima-grade hydrochloric (37%, Seastar Chemicals Inc, Canada) and trace-metal grade hydrofluoric (47–51%, Seastar Chemicals Inc, Canada) acids were used as such. Water was purified (resistivity $\geq$ 18.2 MΩ cm) in a Milli-Q Element water purification system (Millipore, France). Purissima grade acetone, ultrapure 9.8 M H_2O_2 and dimethylglyoxime (DMG) were purchased from Sigma Aldrich (Belgium). All the Teflon® recipients, disposable plastic tubes and pipette tips used for the sample preparation were additionally cleaned by soaking in 10% pro-analysis HCl under class-10 clean lab conditions for 48 h. 1000 mg ml^{-1} single-element stock solutions were acquired from Merck (Darmstadt, Germany), PlasmaCAL (Quebec, Canada), Inorganic ventures (Christiansburg, Virginia, USA) and Alfa Aesar GmbH (Karlsruhe, Germany).

Four iron meteorite specimens (IVB-an Chinga, IIB Sikhote-Alin, IIE Elga and IIC Darinskoe) were obtained from the Central Siberian Geological Museum, V. S. Sobolev Institute of

 This journal is © The Royal Society of Chemistry 2015

Published on 22 May 2015. Downloaded by Universiteit Gent on 16/06/2015 13:15:23.

Geology and Mineralogy, Russia, while IAB-MG Canyon Diablo was obtained from a commercial meteorite dealer. For three of these materials (Sikhote-Alin, Chinga and Canyon Diablo), information on their Ni isotopic composition were published in previous studies, allowing cross-validation of the results obtained in this work. Terrestrial mafic rock reference materials were used to expand the validation of the isolation procedure. These geological reference materials (GRMs) include the basalts BHVO-1, BHVO-2 and BIR-1, peridotite PCC-1, diabase DNC-1 and dunite DTS-1 from the United States Geological Survey (USGS, USA), ultramafic rock OKUM from Geosciences Laboratories (Sudbury, Ontario, Canada), basalt JB-1b and peridotite JP-1 from the Geological Survey of Japan (GSJ) and basalt BE-N and iron formation IF-G from the Centre de Recherches Pétrographiques et Géochimiques (CRPG, France). Reference materials of iron (NBS 365, NBS 461) and alloyed steel (NBS 19g, NBS 125b, NBS 362, NBS 1286) from the National Institute of Standards and Technology (NIST, USA) with a Ni content varying from 0.04 to 2.8 wt% were used to emulate the behavior of the matrix of iron meteorites in the ion exchange separation experiments.

Digestion

Iron meteorite fragments were cut from the bulk mass with a diamond disk saw. To avoid surface contamination effects, visibly altered (*i.e.* oxidized) surfaces were cleaned with silicon carbide sandpaper, subsequently etched with dilute HNO_3 in an ultrasonic bath and finally rinsed with ethanol and dried. Fragments of about 100 mg were weighed and transferred into 15 ml Savillex Teflon® beakers and digested in 4 ml of freshly prepared *aqua regia* (1 : 3 HNO_3 : HCl). For that purpose, the closed vessels were heated at 90 °C during 72 hours. Digestion of silicate samples was performed using a two-step microwave-assisted acid digestion in an MLS-1200 MEGA Microwave digestion system (Milestone, Italy). Each step consists of 30 minutes of heating in a Teflon® vessel at the maximum power of 650 W. First, a mixture of HF : HNO_3 (2.5 ml : 5 ml) was used to dissolve a weighed amount of geological reference material (GRM) powder of about 150 mg. After evaporation to incipient dryness (90 °C), the digestion was continued using the same program with 6 ml of *aqua regia*. After cooling down, the vessels were opened and the solutions were evaporated to incipient dryness at 90 °C. The residues were redissolved in 0.4 ml of concentrated HCl and evaporated to incipient dryness again. The last step was repeated twice. Finally, the residues were redissolved in the corresponding medium for chromatographic isolation of Ni.

Isolation

Ni isolation was carried out in a 3-step ion exchange chromatographic procedure. In a first step, Ni is separated from the main part of the matrix. Two additional steps are subsequently applied to separate Ni from Ti, Fe and Zn. A summary of the Ni ion-exchange isolation procedure is provided in Table 1.

Step 1: for the first step of the chromatographic isolation procedure, 2.5 ml of Dowex 50WX4 resin (200–400 mesh) were loaded into a 2 ml polypropylene column with an inner diameter of 8 mm (Eichrom Technologies, France). The resin was washed with 10 ml of H_2O, 10 ml of 6 M HCl and conditioned using 10 ml of 0.6 M HCl–90% acetone (a mixture of 0.5 ml of 12 M HCl, 0.5 ml of MQ-water and 9 ml of acetone). The sample was loaded onto the column in 10 ml of 0.6 M HCl–90% acetone. The column was then washed with 35 ml of 0.6 M HCl–90% acetone and 10 ml of 0.6 M HCl–95% acetone. Ni was eluted with 6 ml of 0.6 M HCl–95% acetone–0.1 M DMG and collected into a 15 ml Savillex Teflon® beaker. The target fraction was evaporated to dryness. The organic residue in the resulting fraction was destroyed *via* repeated oxidation by concentrated acids. First, 0.3 ml of 14 M HNO_3 and 0.1 ml of H_2O_2 were added and the closed beaker was heated at 140 °C for 3 h, and the resulting digest was evaporated to dryness. This step was repeated twice and alternated with 15 min of ultrasonification. The decomposition of organic material was completed with 0.4 ml of *aqua regia* at 140 °C for 3 hours, and the digest was evaporated to dryness. The residue was redissolved in 0.1 ml of 12 M HCl and again evaporated to dryness in order to eliminate possible nitride ions in the second ion exchange step of the Ni isolation procedure. All the evaporations were done at 90 °C, apart from evaporation of the acetone fractions, performed at 80 °C.

Step 2: 1 ml of Eichrom 1X8 anion-exchange resin (100–200 mesh) was loaded into a 2 ml polypropylene column with an inner diameter of 0.8 cm (Eichrom Technologies, France). The resin was washed with 10 ml of H_2O, 5 ml of 1 M HNO_3 and 5 ml of 6 M HCl before conditioning using 5 ml 0.5 M HF–1 M HCl. The sample was loaded onto the column in 5 ml of 0.5 M HF–1 M HCl medium. Ni starts to elute immediately and was quantitatively washed off with an additional 4 ml of 0.5 M HF–1 M HCl and collected in a Savillex Teflon® beaker. The Ni fraction was evaporated, the residue redissolved in 0.1 ml of 12 M HCl and evaporated to dryness again to eliminate fluorides.

Step 3: a similar Eichrom columns was loaded with 1 ml of Eichrom 1X8 anion exchange resin (100–200 mesh). The resin was washed with 10 ml of H_2O, 5 ml of 1 M HNO_3, and conditioned using 5 ml of 6 M HCl. The sample was loaded onto the column in 1 ml of 6 M HCl medium. With an additional 5 ml of 6 M HCl, Ni was eluted quantitatively in a Savillex Teflon® beaker and evaporated to dryness. The residue was dissolved in 0.1 ml of 14 M HNO_3 and evaporated to dryness again. The latter was repeated twice to eliminate the chlorides. Finally, the residue was dissolved in 3% HNO_3 for ICP-MS measurements.

An aliquot from the final fraction was taken for elemental analysis, while the main fraction was used for Ni isotopic analysis. The last two stages of the Ni isolation procedure were carried out under class-10 clean lab conditions to prevent airborne contamination.

Instrumentation

To record the elution profiles of the single Ni isolation steps, GRMs and synthetic mixtures of mono-element standard solutions were processed following the procedures described above. Element concentrations in the individually collected fractions

Published on 22 May 2015. Downloaded by Universiteit Gent on 16/06/2015 13:15:23.

Table 1 Summary of the Ni ion-exchange isolation procedure

Column 1 (2.5 ml Dowex 50W-X4 200–400 mesh)		
Sample load	10 ml	0.6 M HCl–90% acetone
Matrix wash off	35 ml	0.6 M HCl–90% acetone
	10 ml	0.6 M HCl–95% acetone
Ni collection	6 ml	0.6 M HCl–95% acetone–0.1 M DMG
Column 2 (1 ml Eichrom 1X8 100–200 mesh)		
Sample load, Ni collection	5 ml	0.5 M HF–1 M HCl
Ni collection	4 ml	0.5 M HF–1 M HCl
Column 3 (1 ml Eichrom 1X8 100–200 mesh)		
Sample load, Ni collection	1 ml	6 M HCl + 0.01% H_2O_2
Ni collection	4 ml	6 M HCl + 0.01% H_2O_2

were determined using a Thermo Scientific Element XR sector field ICP-MS instrument *via* external calibration. Rh was relied on as an internal standard. Medium ($m/\Delta m = 4000$) and high ($m/\Delta m = 10\,000$) mass resolution settings were used to resolve interferences.

All target (Ni), and the corresponding leading and tailing chromatographic fractions of the samples selected for Ni isotope characterization were first analyzed for their element composition to ensure full Ni recovery and adequate separation from interfering elements. For this purpose, a Thermo Scientific XSeries II quadrupole-based ICP-MS instrument was used. External calibration was used for this purpose with Rh as an internal standard.

Isotope ratios were measured using a Thermo Scientific Neptune multi-collector ICP-MS unit in medium resolution mode (see Table 2). Samples and standards were presented in 3% HNO_3 solution with a Ni concentration of 1000 μg l^{-1}. The instrumental background originating from the Ni cones was insignificant compared to the signal of samples (<10^{-2} V and 15 V respectively). Each sample was measured 2–3 times during a daily sequence to improve the precision. Ni isotope ratios are expressed relatively to the NIST SRM 986 Ni isotopic reference material (NIST, USA). 10^{12} Ω amplifiers are used for the least intense signals to improve counting statistics.

Correction for instrumental mass discrimination

Correction for instrumental mass discrimination was performed *via* internal correction, relying on (a) the $^{63}Cu/^{65}Cu$ isotope ratio of an admixed in-house Cu isotopic standard, or (b) the $^{62}Ni/^{58}Ni$ isotope ratio of the sample itself. These corrected ratios are indicated hereafter as $(^{x}Ni/^{58}Ni)_{Cu\ corr}$ and $(^{x}Ni/^{58}Ni)_{Ni\ corr}$, respectively. The latter approach not only corrects for instrumental mass discrimination, but also cancels out any natural or artificial mass-dependent Ni isotope fractionation experienced by the sample during its evolution or sample preparation.[20,23] The Russell (kinetic) law[34] was found suitable for the correction of mass bias, with the version revised by Baxter found most successful.[35] For the details on the evaluation of the different correction laws, the reader is referred to the ESI.† Finally, sample-standard bracketing was applied to correct for minor drift of instrumental parameters. Isotope ratios internally corrected with Cu are reported as the relative differences of the Ni isotope ratio ($\delta^{x/58}Ni$) relative to that in the NIST SRM 986 Ni isotopic reference material, measured within the same sample-standard bracketing sequence:

$$\delta^{x/58}\mathrm{Ni} = \left[\frac{(^{x}\mathrm{Ni}/^{58}\mathrm{Ni})_{\mathrm{Cu\ corr,\ smp}}}{(^{x}\mathrm{Ni}/^{58}\mathrm{Ni})_{\mathrm{Cu\ corr,\ NIST986}}} - 1\right] \times 1000 \qquad (1)$$

Hereafter, these mass-dependent variations are reported in permil (‰) and the corresponding results are called mass-dependent. When reporting isotope ratios, internally corrected by $^{62}Ni/^{58}Ni$, to cancel out all natural mass-dependent fractionation effects, the $\varepsilon^{x/58}Ni$ notation is used to distinguish these results from those normalized by Cu correction. As these deviations with respect to the isotopic reference material are generally smaller, they are reported in pptt (part per ten thousand) and the corresponding results are called non mass-dependent:

$$\varepsilon^{x/58}\mathrm{Ni} = \left[\frac{(^{x}\mathrm{Ni}/^{58}\mathrm{Ni})_{\mathrm{Ni\ corr,\ smp}}}{(^{x}\mathrm{Ni}/^{58}\mathrm{Ni})_{\mathrm{Ni\ corr,\ NIST986}}} - 1\right] \times 10\,000 \qquad (2)$$

Results and discussion

Mathematical corrections of isobaric interferences

The Thermo Neptune multi-collector ICP mass spectrometer used is equipped with 9 Faraday cups, which is theoretically sufficient to monitor all Ni isotopes simultaneously, the Cu isotopes for the internal correction, as well as ^{56}Fe and ^{66}Zn for mathematical correction of isobaric interferences. However, due to instrument limitations, the mass range of interest, ranging from 56 to 66 amu cannot be covered simultaneously. As a result, a dynamic mode of acquisition was applied, and the relevant isotopes of Fe and Zn were not monitored simultaneously. The intensity of the ^{56}Fe signal was always found to be very low compared to that of the Ni isotopes. The ^{56}Fe signals of samples and bracketing standards were found to be similar (about 10^{-2} V). For comparison, intensities for ^{58}Ni were typically around of 15 V. Typically, the ^{66}Zn signals for the samples

 This journal is © The Royal Society of Chemistry 2015

Published on 22 May 2015. Downloaded by Universiteit Gent on 16/06/2015 13:15:23.

Table 2 Instrument settings, data acquisition parameters and multi-collector detector configuration for the Thermo Scientific Neptune MC-ICP-MS instrument used for Ni isotopic analysis

Instrument settings		
RF power[a], W		1250
Gas flow rates[a], l min^{-1}	Cool	15
	Auxiliary	0.8
	Nebulizer	0.98
Sampler cone		Ni: 1.1 mm aperture diameter
Skimmer cone		Ni, H-type: 0.8 mm aperture diameter
Sample uptake		Pumped *via* peristaltic pump, 0.1 ml min^{-1}
Nebulizer		Concentric, 100 μl min^{-1}
Spray chamber		Double, cyclonic and Scott-type sub-units
Resolution mode		Medium[b]
Data acquisition		
Mode		Dynamic (^{56}Fe and ^{66}Zn are measured non-simultaneously for mathematical correction[b])
Idle time, s		3
Integration time, s		4.194
Number of integrations		3
Number of blocks		4
Number of cycles per block		3

Cup configuration[c]

Cup	L_4	L_2	L_1	C	H_1	H_2	H_3
Amplifier	10^{11} Ω	10^{11} Ω	10^{11} Ω	10^{12} Ω	10^{11} Ω	10^{12} Ω	10^{11} Ω
1st line	^{58}Ni, ^{58}Fe	^{60}Ni	^{61}Ni	^{62}Ni	^{63}Cu	^{64}Ni, ^{64}Zn	^{65}Cu
2nd line				^{56}Fe			
3rd line				^{66}Zn			

[a] Parameters optimised on a daily basis for highest sensitivity and stability. [b] Δm for pseudo-high resolution in MC-ICP-MS is defined as the mass difference between $m_{5\%}$ and $m_{95\%}$.corresponding to 5% and 95% of the signal intensity level on the plateau, respectively. A resolving power of 7400 was measured using the ^{238}U signal in MR mode. The resolving power as calculated following this definition exceeds the mass resolution calculated as m/the peak width at 5% peak height by more than a factor of two.[33] [c] See 'Results and discussion' section for further information.

were similar to those obtained for the bracketing standards (<10^{-3} V), but occasionally reached intensities 2–5-fold higher. Mathematical corrections for isobaric interferences affecting ^{58}Ni and ^{64}Ni were based on non-simultaneous measurement of ^{56}Fe and ^{66}Zn, the Russell exponential law, and a mass bias correction factor calculated using the Cu internal standard. For this purpose, standards with natural Fe, Cu and Zn isotopic composition were measured to calculate the linear correlation parameters of the fractionation coefficients f_{Fe}–f_{Cu} and f_{Zn}–f_{Cu}.[36] These parameters were then used to calculate the mass-biased ^{66}Zn/^{64}Zn and ^{58}Fe/^{56}Fe ratios for the samples, and finally, these ratios were used to correct the ^{58}Ni and ^{64}Ni intensities for isobaric overlap resulting from the trace levels of Fe and Zn, respectively. The effect of the mathematical correction on ^{58}Ni was always insignificant, as this is the most abundant isotope of Ni, interfered by the least abundant isotope of Fe. On the other hand, the effect of ^{64}Zn on ^{64}Ni is substantial. Fig. 1(A) shows the data for NIST SRM 986, suffering from a background Zn contamination (originating from the different autosampler vials) before and after the mathematical correction. As ^{64}Ni was found to be very sensitive to background Zn interference, the levels of Zn which could be corrected for mathematically were determined experimentally. Fig. 1(B) shows the ^{64}Zn-corrected results for the NIST SRM 986 Ni isotopic reference material (1 μg g^{-1}), when doped with different concentrations of Zn. These plots show that Zn background levels of up to 10 ng g^{-1} can be corrected for without significant deterioration in the precision of the ^{64}Ni/^{58}Ni ratio. At Zn levels higher than 10 ng g^{-1}, the spread in the ^{64}Ni/^{58}Ni ratios increases with more pronounced deviations from the NIST SRM 986 reference line.

The concentration level of Zn at which mathematical correction can be applied is also limited by the non-simultaneous character of the ^{64}Ni and ^{64}Zn monitoring. Based on our experiments, the number of lines in a dynamic mode does not affect the precision of the Ni isotope ratio measurements themselves, as all of the Ni isotopes are measured simultaneously (1st line). The precision deteriorates only when both (a) the non-simultaneously measured ^{66}Zn intensity is included in the calculations, and (b) the Zn background concentration is higher than the limit determined.

Other interferences

At the level of natural variation of Ni isotope ratios studied, many elements, present in the natural matrices, can give rise to spectral interferences that affect the results of Ni isotope ratio measurements. The medium resolution mode ($m/\Delta m = 7400$) of the Thermo Neptune was used to resolve most of these species. Among all the elements evaluated, only the effect of Ti was

Published on 22 May 2015. Downloaded by Universiteit Gent on 16/06/2015 13:15:23.

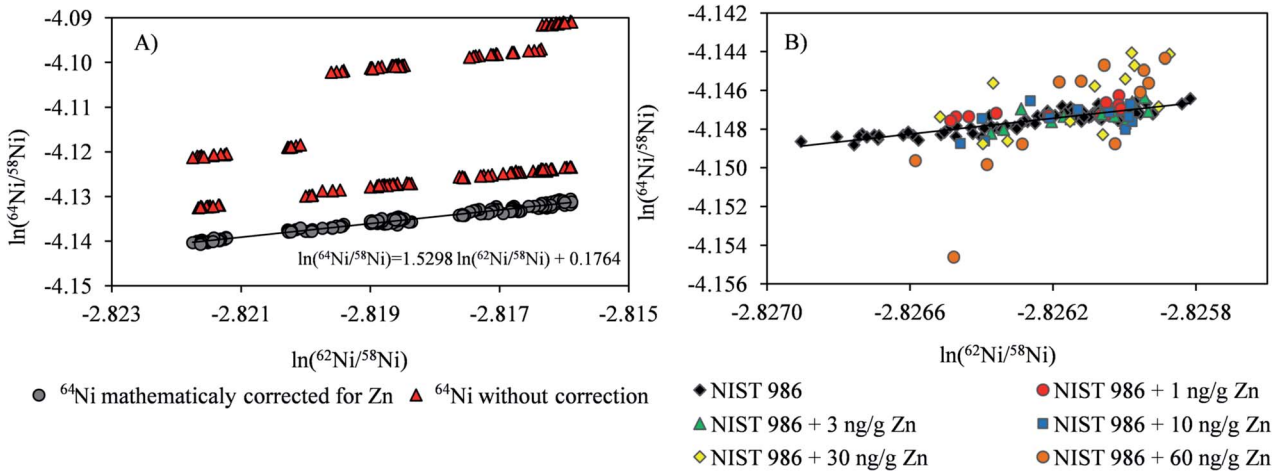

Fig. 1 (A) – The effect of a mathematical correction for the $^{64}Zn/^{64}Ni$ isobaric interference. Red triangles represent uncorrected data suffering from a background Zn contamination measured in different autosampler vials. (B) – The effect of Zn on the $^{64}Ni/^{58}Ni$ isotope ratio after the mathematical correction. Different amounts of Zn are added to the NIST SRM 986 and the data mathematically corrected for ^{64}Zn are plotted in the 3-isotope plot.

found to be significant, even when its concentration is below that of the target analyte Ni. For a more detailed description of the effect of spectral interferences, the reader is referred to the ESI.†

Thus, Ti and Zn are the most critical interfering elements and these need to be reduced to background levels during sample preparation. The presence of other interfering elements in amounts lower than that of Ni will not affect the measurement of Ni isotope ratios.

Development of the ion-exchange chromatographic isolation of Ni

The earliest reports on Ni isotopic analysis relied on the extraction of Ni using a dimethylglyoxime (DMG) solution – a highly selective compound that binds Ni into a chelate complex.[37,38] Despite the high efficiency of such a separation, sufficiently low blank levels cannot be ensured.

Later works on Ni isolation procedures were based on a combination of cation and anion exchange chromatographic separation steps.[6,24] This approach relies on the fact that Ni, in contrast to many other elements, does not form chloro-complex anions. As a result, Ni can be separated from chloro-complex-forming elements by binding to a cation exchanger. Similarly, anion exchange chromatography can be used with a reversed elution order. Attractive by its simplicity, the potential of this approach to separate Ni from alkali and alkaline earth metals is compromised by the limited differences in the distribution coefficients (K_d) and the corresponding necessity of a highly efficient column with a high number of theoretical plates.[39] Complete separation of Ni from abundant elements that possess chemical properties very similar to those of Ni, such as Co, and some transition elements that can be present in a diversity of chemical forms in the solution (*e.g.*, Cr, V, Ti) is hard to achieve. Nevertheless, this separation approach can be used efficiently when these limitations are properly addressed (*e.g.*, for the analysis of iron meteorites).

Application of organic solvents as a separation medium increases the peak resolution of the cation exchange column and thus, improves the separation factors.[40] A general trend is that Ni distribution coefficients in a weak HCl–strong cation exchange system increase when the concentration of organic solvent is increased, while those for Fe, Co and Zn decrease. According to the K_d values published, separation of Ni from Al, Ca, Co, and K is feasible when using 0.5 M HCl in 90% acetone.[41] But, this approach does not solve the problem of Ni separation from Cr, Mg, Na and Ti, elements which are abundantly present in meteorite matrices. Therefore, separation in HCl–acetone medium on a cation exchange resin was combined with additional anion exchange columns to isolate Ni from iron meteorites and chondrites and determine its isotopic composition.[42–44]

A solution to the insufficient selectivity described above lies in the simultaneous use of DMG and ion exchange chromatography. This can be achieved by using the commercially available Ni-specific Eichrom resin, containing DMG fixed in its pores,[8,19,38,45] or the conventional 50W-X4 strong cation exchanger in a weak HCl–acetone–DMG medium.[23,26,31] The latter method was first described by Wahlgren *et al.*[46] and later by Victor.[47] At the first stage of this separation, elements that form chloro-complex anions and do not show affinity to the cation exchanger in HCl–acetone medium are eluted with 0.6 M HCl–90% acetone. At the same time, other elements (*e.g.*, Al, Ca, Na, K, Mg, see Strelow *et al.*[41] for K_d) are retained on the resin, together with Ni. A solution of DMG in acetone is then used for a selective elution of the retained Ni. K_d of Ni decreases from 250 down to 4 when adding 0.1 M DMG to 0.6 M HCl–95% acetone.[47] The presence of Ti in the final elution of this separation is described in literature, and for its removal, an additional column is needed to further purify the Ni fraction.[23,26,31] Also, blank levels of organic solvents cannot be as low as those

 This journal is © The Royal Society of Chemistry 2015

Published on 22 May 2015. Downloaded by Universiteit Gent on 16/06/2015 13:15:23.

achieved in aqueous solutions. Finally, it needs to be considered that working with acetone brings about additional technical challenges – evaporation of the solvent, the low viscosity, acetone polymerization in acid, and the formation of air bubbles in the column. Another drawback is the presence of organic material in the final elution. This can affect Ni isotope measurements in a non-spectral way or lead to complexation of Ni cations, which could corrupt subsequent ion exchange separation steps. Therefore, this organic material has to be decomposed effectively before the next separation step or MC-ICP-MS isotopic analysis take place.

An improvement of the abovementioned method for Ni purification was described by Gall *et al.*[31,48] This approach minimizes the amounts of acetone and DMG used with the aim of keeping the post-purification treatment of the sample as limited as possible. For this purpose, elements such as Al, Cr, Fe, and Ti are first eluted off as oxalic complexes with an oxalic acid–HCl solution, followed by the application of HCl–acetone to wash off Cd, Cu, Mn, Sn, and Zn. In a final step, Ni is collected in an HCl–acetone–DMG medium.

Another approach for additional Ni fraction purification, based on the original separation of Strelow[49] was proposed by Gall *et al.*[31] Ni is loaded in a dilute solution of di-ammonium citrate and NH_4OH on a cationic exchanger, and the excess of ammonia complexes Ni and some other electronegative divalent ions and binds these to the cation exchanger. At the same time, alkali and alkaline earth elements and other cations abundant in geological materials tend to form citrate complexes, which show no affinity towards the resin. As a result, Ni can be separated from the geochemically abundant elements – Al, Ca, Cr, Fe, Ti, Mg, and V.

Based on the literature available, cation and anion exchange chromatographic steps were combined in this work (see Table 1 for a summary) in order to ensure isolation of Ni from the matrix and interfering elements and guarantee that on-column isotope fractionation does not affect the final result. The first step comprises cation exchange separation in 0.6 M HCl–95% acetone–0.1 M DMG to separate Ni from most of the matrix elements and to reduce the concentration of potentially interfering elements to background levels. An elution profile is shown in Fig. 2 (the final fractions were eluted with 6 M HCl to calculate the recoveries of elements bound to the resin). Application of the 50W-X4 cation exchange resin (4% cross-linkage) was found advantageous compared to similar resins with higher cross-linkage. Strong tailing of the Ni peak was observed when using 50W-X8 (8% cross-linkage). 16 ml of 0.6 M HCl–95% acetone–0.1 M DMG were needed to obtain quantitative Ni recovery with the latter resin, compared to 6 ml in the case of 50W-X4 with similar mesh size. The elution profiles of synthetic mixtures of single-element standards, GRMs and iron meteorites all show similar peak positions. This demonstrates the absence of matrix effects on the elution behaviour.

After this first separation step, the level of most interfering elements decreases below the limits appropriate for Ni isotope ratio determination (below a 1 : 1 ratio relative to Ni, as documented in the previous section). Only the chromatographic peaks of Ti, Cr and minor peaks of V and Al overlap with the

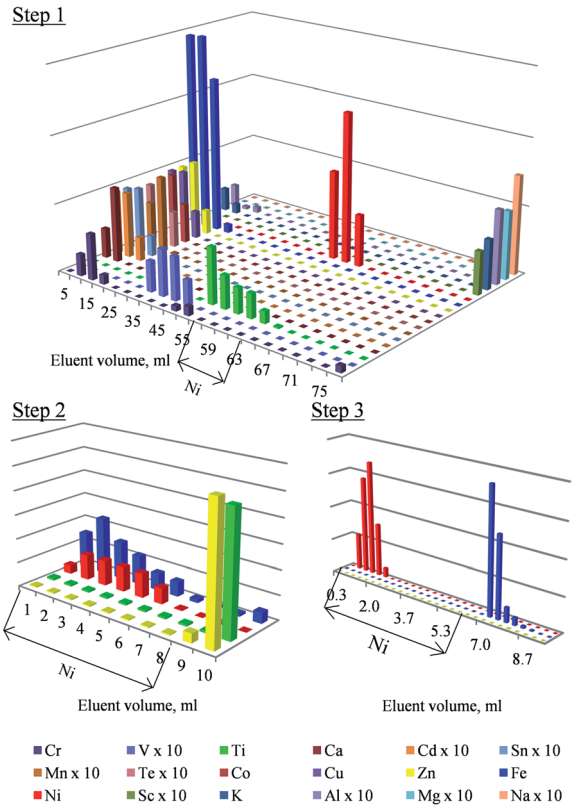

Fig. 2 Elution profiles for Ni ion-exchange isolation.

peak of Ni in the elution profiles. As Ti was found to be one of the elements significantly affecting Ni isotopic analysis, the use of a second column for cleaning the Ni fraction is crucial.

Crushing and removing the organic residue remaining after the first elution was found critical for further isolation. This can be achieved *via* repeated digestion by concentrated inorganic acids and H_2O_2 at high temperature. Such treatment converted the brown residue into a tiny green-blue dot.

The second column is based on anion exchange chromatography in a HCl–HF mixture medium and aimed at Ni separation from Ti. HF strongly complexes Ti and Zn, such that these elements are strongly adsorbed onto the anion exchanger.[50] As a result, these elements can be separated from Ni that does not form fluoro-complex anions and hence, does not show significant absorbance. With increasing HCl concentration, the adsorption of Ti becomes negligible. At the same time, Fe is only adsorbed in HCl–HF medium at higher HCl concentrations, and thus, Ni cannot be separated from Fe during separation of Ni from Ti and Zn. The elution profile obtained under the optimized conditions is shown at Fig. 2.

A third chromatographic column (see Table 1) is needed to achieve sufficiently low background levels of Fe and Zn. Although these elements are efficiently separated from Ni in the first column step, sufficiently low blanks cannot be obtained because of the use of organic solvents and DMG. The separation presented here is based on the use of anion exchange chromatography (see Fig. 2 for elution profiles).[51] Fe and Zn form anionic chloro-complexes that are strongly bound to the

Published on 22 May 2015. Downloaded by Universiteit Gent on 16/06/2015 13:15:23.

exchanger, while Ni is eluted. Small amounts of H_2O_2 are added to prevent Fe from being reduced from Fe(III) to Fe(II), which cannot form chloro-complex anions. Ni recoveries were quantitative for the second and third columns.

Element-to-Ni mass ratios were measured after isolation of Ni from geological, iron and low-alloyed steel reference materials, which approximate the matrix of iron meteorites. The abundances of the interfering elements after isolation were found to be much lower than the experimentally determined tolerance limits. The characteristics of the complete isolation method are summarized in the ESI.† If trace levels of Ti (Ti : Ni ratio higher than 10^{-3}) were found present after Ni isolation from GRMs, Ni isotope ratios measurements were performed using high mass-resolution mode at the cost of deteriorated precision on $^{64}Ni/^{58}Ni$ isotope ratio.

The recoveries for Ni, calculated for the complete isolation procedure, including the three ion exchange columns and all of the intermediate sample treatment procedures are 81–87% and 82–106% for iron and geological matrices, respectively. The minimum recovery calculated for the total procedure is equivalent to 93% recovery for each of the three ion exchange separation steps.

The application of anion exchange separation after the first column has the important advantage that the chemical forms of Ni present have almost no affinity to the resin. It not only makes these separations faster, improves recovery, but also prevents losses of Ni, leading to fractionation. Thus, in the case of incomplete DMG decomposition, neutral Ni complexes will be eluted from the 2nd and 3rd columns together with Ni^{2+}. Another advantage of anion exchange is that on-column mass-dependent fractionation is self-evidently absent as this can only occur for an element showing affinity towards the resin.

Studies of on-column fractionation of Ni

To evaluate the effect of on-column isotope fractionation, a digest of isotopic reference material NIST SRM 986 was loaded on the first column and the band of Ni was collected in aliquots of 0.5 ml in Savillex Teflon® beakers. The isotopic composition of Ni in these separate fractions was then measured relative to NIST SRM 986. $\delta^{x/58}$Ni values along the elution profile of the first column are shown in Fig. 3.

It can be seen that the leading fractions of the Ni elution band are isotopically lighter, while the tailing fractions are heavier. This on-column isotope fractionation can be corrected for when using a pair of Ni isotopes. Isotope fractionation on the first column is purely mass-dependent and fits a first order mass-dependent fractionation law for isotope partitioning at equilibrium, according to the method described by Young *et al.* (*cf.* Fig. 4).[52,53] The β fractionation exponent was extracted from the experimental data for on-column Ni isotope fractionation and compared to the theoretically expected β parameters for equilibrium and kinetic mass-dependent fractionation processes. β is a fractionation exponent coupling isotope fractionation factors $\alpha_{x/58}$ as:

$$\alpha_{62/58} = \alpha_{60/58}{}^{\beta}; \tag{3}$$

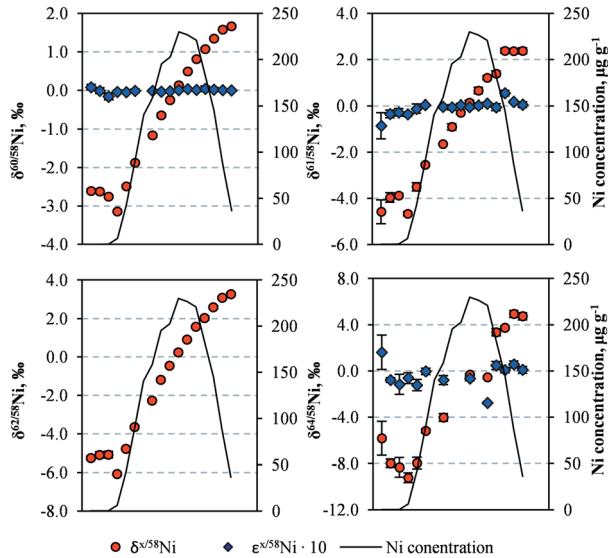

Fig. 3 Profiles of $\delta^{x/58}$Ni and $\varepsilon^{x/58}$Ni along the Ni elution band from the first column of the chromatographic isolation protocol.

Following Wombacher and Rehkamper,[53] the theoretical equilibrium and kinetic β factors are calculated as:

$$\beta_{eq} = \frac{\left(\frac{1}{m_{58}} - \frac{1}{m_{62}}\right)}{\left(\frac{1}{m_{58}} - \frac{1}{m_{60}}\right)} \tag{4}$$

$$\beta_{kin} = \frac{\ln\left(\frac{m_{58}}{m_{62}}\right)}{\ln\left(\frac{m_{58}}{m_{60}}\right)} \tag{5}$$

$$\beta_{pow} = \frac{(m_{58} - m_{62})}{(m_{58} - m_{60})} \tag{6}$$

The maximum spread of on-column isotopic enrichment found for the first column mounted up to ±4‰ for $\delta^{60/58}$Ni, implying the need for recoveries close to 100% to avoid on-column bias when natural mass-dependent isotope fractionation needs to be studied. Hence, a higher volume of eluent than strictly necessary was always used to wash Ni from the first column. A Ni standard was processed together with each batch of samples studied, and the results obtained were compared to a non-processed standard to detect any isotope fractionation occurring during sample preparation.

Similar experiments were carried out for the 2nd and 3rd anion exchange columns, but no on-column fractionation effects were detected. This can be explained by the simple fact that Ni shows no significant affinity to the anion exchanger, and thus, there is no chemical interaction that can fractionate the Ni isotopes.

Precision

The precision attainable with the method for Ni isotopic analysis used defines the applications within reach. Chronological

 This journal is © The Royal Society of Chemistry 2015

Published on 22 May 2015. Downloaded by Universiteit Gent on 16/06/2015 13:15:23.

applications require the highest precision, as the uncertainty on the isotope ratio measurement is translated *via* error propagation into millions years of uncertainty on the final radioisotopic date.[54]

The reproducibility of the relative isotope ratio differences attained was calculated *via* repeated measurement of digested Sigma Aldrich high-purity Ni metal during all of the measurement sessions throughout this work. The overall reproducibility achieved (2 SD, $n = 14$) is 0.033‰, 0.045‰, 0.071‰ and 0.51‰ for $\delta^{60/58}$Ni, $\delta^{61/58}$Ni, $\delta^{62/58}$Ni and $\delta^{64/58}$Ni, respectively. Another estimation of the overall reproducibility was done by repeated measurement of a real sample, since small deviations can potentially be introduced during the chemical isolation of Ni. In this work, reproducibilities of 0.048‰, 0.14‰, 0.065‰ and 0.39‰ were found for $\delta^{60/58}$Ni, $\delta^{61/58}$Ni, $\delta^{62/58}$Ni and $\delta^{64/58}$Ni, respectively, for repeated measurements of the PCC-1 peridotite GRM (2 SD, $n = 8$). Previous works[6,8,19,31] have reported reproducibilities between 0.034 and 0.08‰ for $\delta^{60/58}$Ni. These figures of merit need to be compared with the natural isotopic variation for Ni. The spread of $\delta^{60/58}$Ni within 150 meteorites of different groups reported by Moynier *et al.*[6] is on the order of 0.20‰ (2 SD). Within groups of meteorites, even smaller deviations of 0.06‰ have been reported.[19] As such, the reproducibility obtained in this work should at least be enough to resolve different groups of meteorites.

When correcting Ni isotope ratio data internally by ^{62}Ni/^{58}Ni to reveal the non mass-dependent effects, the reproducibility attained is 0.53 pptt, 1.1 pptt, and 6.8 pptt for $\varepsilon^{60/58}$Ni, $\varepsilon^{61/58}$Ni and $\varepsilon^{64/58}$Ni, respectively (2 SD *via* repeated measurement of a digested Sigma Aldrich high purity Ni metal, $n = 14$). These results are slightly higher than those reported by Quitté *et al.*[24] (0.3 pptt and 0.6 pptt for $\varepsilon^{60/58}$Ni and $\varepsilon^{61/58}$Ni, respectively). For repeated measurements of PCC-1 peridotite, reproducibilities of 0.25 pptt, 1.1 pptt and 1.3 pptt were found for $\varepsilon^{60/58}$Ni, $\varepsilon^{61/58}$Ni and $\varepsilon^{64/58}$Ni, respectively (2 SD, $n = 8$). These figures are similar to the spread in the natural variation of $\varepsilon^{60/58}$Ni found by Quitté *et al.* (0.53 pptt)[24] and Cook *et al.* (0.3 pptt)[42] in a diversity of iron meteorites. Because the differences studied are small, the investigation of non mass-dependent effects affecting Ni isotope ratios remains highly challenging.

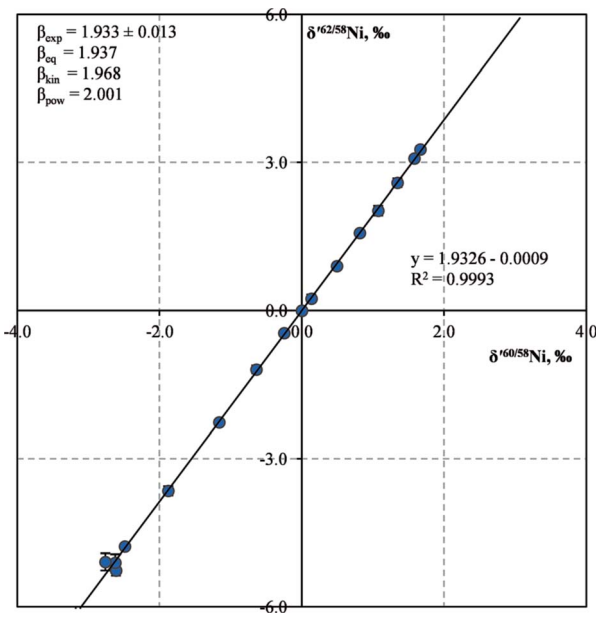

Fig. 4 Three-isotope plot constructed using the approach described by Young *et al.*[52,53] and the experimental Ni isotope ratio data for the Ni elution profile of the first column. The slope of the regression line is equal to the fractionation exponent β between the isotope ratios. By definition $\delta'^{x/58}\text{Ni} = \ln[(^{x}\text{Ni}/^{58}\text{Ni})_{smp}/(^{x}\text{Ni}/^{58}\text{Ni})_{std}] \times 1000$.

Results

The non mass-dependent Ni isotopic data obtained in this work are presented in Table 3. To obtain these results, all natural mass-dependent contributions to the fractionation are canceled out by an assumed fractionation "law". Taking the associated analytical uncertainties into consideration, none of the results obtained indicates a significant difference with respect to NIST SRM 986. Also when comparing the results to one another, no significant effects can be seen (see Table 3). The precision of $\varepsilon^{64/58}$Ni is compromised particularly by considering the effect of the Zn background in the calculation of the uncertainty budget. This input has a random nature and can be smaller or higher in particular case (*e.g.* BHVO-2 and BIR-1 in Table 3). As such, the applicability of Ni isotope data of iron meteorites for chronological purposes or to assess specific nucleosynthetic contributions remains debatable. Here, it needs to be stressed that available literature data on the non mass-dependent Ni isotopic data of iron meteorites are also not resolvable from NIST SRM 986 within the obtainable level of analytical resolution.

To validate the mass bias correction model used, non mass-dependent $\varepsilon^{60/58}$Ni are plotted *versus* mass-dependent $\delta^{60/58}$Ni in Fig. 5. For the iron meteorites and terrestrial GRMs studied, no significant correlation exists between the mass-dependent and non mass-dependent data, suggesting that natural and instrumental mass-dependent isotope fractionation effects are entirely cancelled out after the correction and no artifacts due to overcorrection are present.

Mass-dependent data are presented in Table 3. $\delta^{60/58}$Ni values vary between −0.069‰ and 0.58‰ for the terrestrial GRMs studied, and between 0.191‰ and 0.408‰ for the iron meteorites studied. In general, the results obtained in this work for the GRMs are in good agreement with those previously obtained using a double spike approach[8,23] (t-test, $t_{exp} < t_{crit}$, $p < 0.05$). The $\delta^{60/58}$Ni result for PCC-1 peridotite is slightly higher than that reported by Gueguen *et al.*[8] The Ni isotopic composition of iron meteorites and terrestrial silicate GRMs indicates the influence of a mass-dependent isotope fractionation process, as the measured $\delta^{x/58}$Ni values follow a linear correlation in three-isotope space (Fig. 6). As the Ni isotopic compositions of meteorites fall within experimental uncertainty onto the terrestrial fractionation line, this suggests a common nature of the Ni source and a similar control by isotope fractionation processes.

Fig. 7 presents the Ni isotopic compositions of 3 separate digestions of the Canyon Diablo IAB-MG iron meteorite. As each

Published on 22 May 2015. Downloaded by Universiteit Gent on 16/06/2015 13:15:23.

Table 3 Non mass-dependent (presented in pptt) and mass-dependent (presented in ‰) Ni isotope ratio data for 5 iron meteorites, 11 GRMs and some literature data for reference. Uncertainty denotes 2 SD. *n* denotes for separate digestions

	$\varepsilon^{60/58}$Ni, pptt	$\varepsilon^{61/58}$Ni, pptt	$\varepsilon^{64/58}$Ni, pptt	$\delta^{60/58}$Ni, ‰	$\delta^{61/58}$Ni, ‰	$\delta^{62/58}$Ni, ‰	$\delta^{64/58}$Ni, ‰	$\varepsilon^{60/58}$Ni, pptt, Ref.	$\varepsilon^{61/58}$Ni, pptt, Ref.	$\varepsilon^{64/58}$Ni, pptt, Ref.	$\delta^{60/58}$Ni, ‰, Ref.
Canyon Diablo[a]	−0.01 ± 0.51	0.21 ± 0.24	−1.7 ± 5.8	0.262 ± 0.026	0.407 ± 0.022	0.523 ± 0.048	0.67 ± 0.44	−0.19 ± 0.23 [24]; 0.06 ± 0.07 [42]	−0.59 ± 0.79 [24]; 0.14 ± 0.58 [42]	0.19 ± 0.8 [42]	
Canyon Diablo[a]	0.20 ± 0.28	0.2 ± 2.2	−1.7 ± 5.6	0.408 ± 0.024	0.63 ± 0.22	0.805 ± 0.046	1.36 ± 0.88				
Canyon Diablo[a]	0.29 ± 0.17	0.33 ± 0.78	0.5 ± 1.5	0.191 ± 0.020	0.30 ± 0.10	0.370 ± 0.064	0.590 ± 0.050				
Sikhote-Alin[a]	0.11 ± 1.4	−0.07 ± 0.88	−1.7 ± 1.6	0.192 ± 0.038	0.29 ± 0.13	0.389 ± 0.099	0.51 ± 1.1	0.33 ± 0.25 [24]	0.27 ± 0.27 [24]	—	
Sikhote-Alin[a]	0.15 ± 0.20	0.7 ± 1.7	−1.0 ± 3.8	0.267 ± 0.031	0.46 ± 0.18	0.513 ± 0.085	0.68 ± 0.44				
Darinskoe ($n = 2$)	−0.14 ± 0.37	−0.4 ± 1.5	−1.4 ± 2.9	0.229 ± 0.040	0.31 ± 0.14	0.478 ± 0.078	0.57 ± 0.41				
Chinga ($n = 2$)	−0.19 ± 0.38	−0.2 ± 1.4	−1.4 ± 4.1	0.222 ± 0.029	0.33 ± 0.13	0.476 ± 0.083	0.77 ± 0.77	0.12 ± 0.17 [24]	0.67 ± 1.23 [24]		
Elga ($n = 2$)	−0.04 ± 0.20	−0.2 ± 1.1	−1.8 ± 3.0	0.238 ± 0.041	0.334 ± 0.085	0.478 ± 0.072	0.62 ± 1.3				
DNC-1 ($n = 5$)	0.07 ± 0.32	0.4 ± 1.4	−2.2 + 5.4	0.188 ± 0.095	0.312 ± 0.070	0.38 ± 0.18	0.16 ± 0.32				0.132 ± 0.056 [8]
PCC-1 ($n = 8$)	−0.13 ± 0.25	0.1 ± 1.1	−0.6 ± 1.3	0.166 ± 0.048	0.25 ± 0.14	0.342 ± 0.065	0.62 ± 0.39				0.11 [31]; 0.119 ± 0.045 [8]
BHVO-2 ($n = 5$)	0.09 ± 0.91	0.0 ± 1.0	−1.9 ± 0.3	0.083 ± 0.019	0.109 ± 0.076	0.164 ± 0.079	−2.2 ± 3.9				0.060 ± 0.050 [31]; 0.006 ± 0.041 [8]; 0.13 ± 0.03 [19]; 0.01 ± 0.02 [12]
BHVO-1 ($n = 2$)	0.15 ± 0.29	0.9 ± 2.2	−0.34 ± 0.96	0.081 ± 0.034	0.19 ± 0.20	0.130 ± 0.093	0.14 ± 0.1				
BE-N ($n = 1$)	0.06 ± 0.56	−0.68 ± 0.27	−0.83 ± 0.86	0.074 ± 0.029	0.043 ± 0.072	0.146 ± 0.059	0.139 ± 0.004				
BIR-1($n = 2$)	−0.01 ± 0.37	0.5 ± 2.6	−2.1 ± 5.6	0.191 ± 0.066	0.33 ± 0.31	0.369 ± 0.088	0.29 ± 0.42				0.120 ± 0.035 [8]
DTS-1 ($n = 2$)	0.31 ± 0.29	0.49 ± 0.70	0.6 ± 2.1	−0.069 ± 0.006	−0.136 ± 0.052	−0.176 ± 0.015	−0.35 ± 0.10				−0.071 ± 0.053 [8]
JB-1b ($n = 1$)	−0.16 ± 0.44	−0.1 ± 3.1	—	0.205 ± 0.017	0.30 ± 0.30	0.394 ± 0.059	−1.4 ± 1.8				
JP-1 ($n = 1$)	−0.15 ± 0.78	−0.9 ± 3.1	—	0.134 ± 0.029	0.217 ± 0.077	0.27 ± 0.16	0.54 ± 0.53				0.100 ± 0.08 [23]
OKUM ($n = 1$)	−0.08 ± 0.81	−1.5 ± 4.0	—	0.58 ± 0.13	0.68 ± 0.13	1.13 ± 0.25	−0.45 ± 0.49				
IF-G ($n = 2$)	−0.0 ± 1.6	−0.0 ± 0.13	0.6 ± 2.8	0.502 ± 0.060	0.753 ± 0.076	0.985 ± 0.087	1.46 ± 0.11				0.455 ± 0.032 [8]

[a] Denotes separate digestions.

This journal is © The Royal Society of Chemistry 2015

Published on 22 May 2015. Downloaded by Universiteit Gent on 16/06/2015 13:15:23.

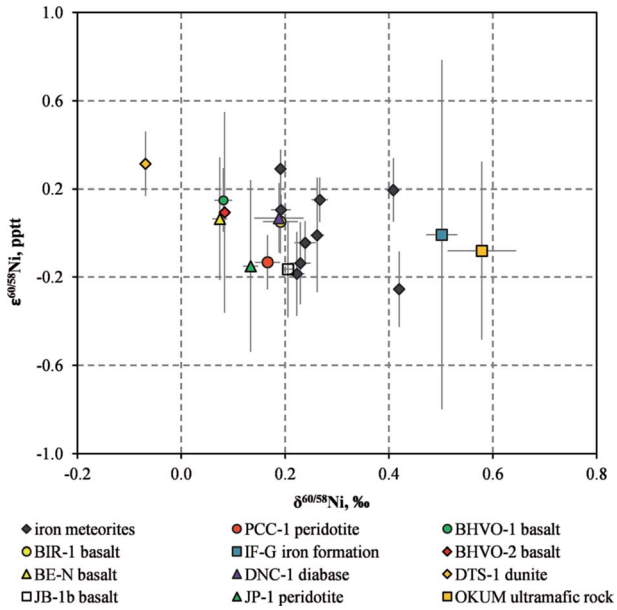

Fig. 5 Plot of the mass-dependent $\delta^{60/58}$Ni values *vs.* the non mass-dependent $\varepsilon^{60/58}$Ni values. All the data couples reported are from the same measurement and the two values are obtained after different correction for mass bias, relying on admixed Cu and one Ni isotope ratio, respectively.

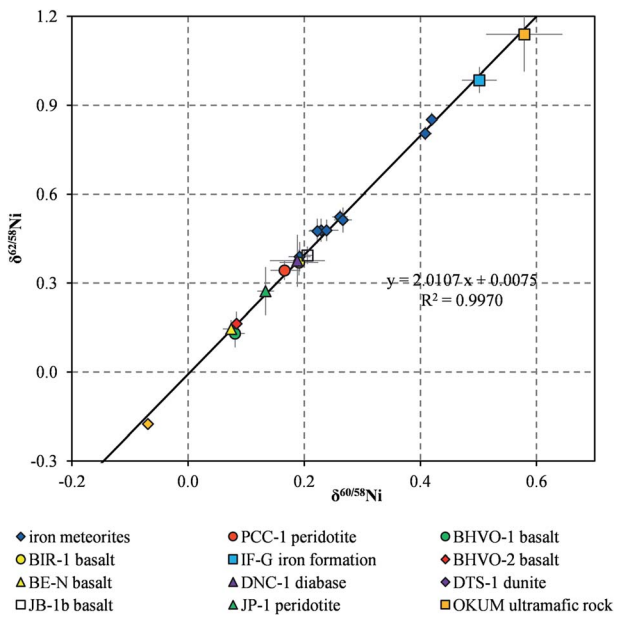

Fig. 6 Three-isotope plot of mass-dependent Ni isotope ratio data for 6 iron meteorites and 11 GRMs.

digestion was processed through the isolation method and measurement protocol twice, the mass-dependent fractionation observed can not result from on-column fractionation or instrumental bias. According to Wasson *et al.*,[55] the IAB meteorite group has a non-magmatic origin and was formed from a chondritic parent body after the rapid cooling of impact-generated melt early in the Solar System evolution. As this type of meteorite has a heterogeneous internal structure,

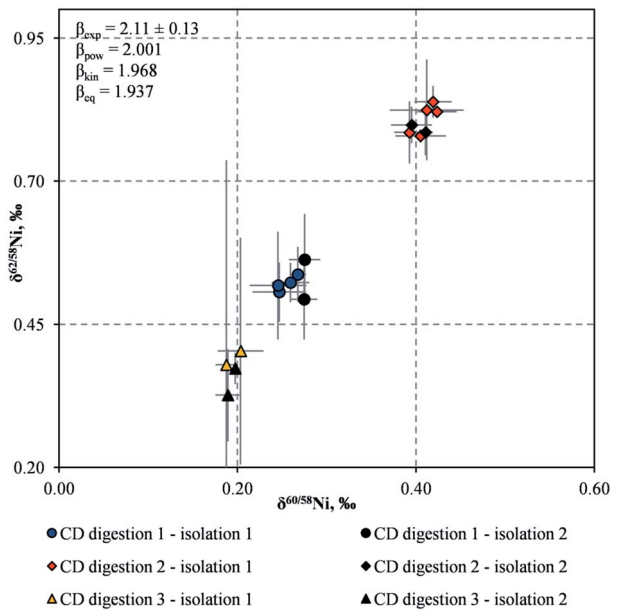

Fig. 7 Three-isotope plot of mass-dependent Ni isotope ratio data for 3 different digestions of the Canyon Diablo IAB-MG iron meteorite.

characterized by different Ni contents (*e.g.*, Ni-rich/poor lamellae, silicate inclusions), the slope of the mass-dependent line in the three-isotope plot likely represents Ni isotope fractionation between petrologic phases of Canyon Diablo. Although the exact spatial connection of the sampled fractions is unclear, these fragments most probably represent kamatite and taenite (Fe/Ni alloys with <10 wt% and 22–77 wt% of Ni, respectively[56]) in different proportions, as non-metal inclusions were avoided during sample preparation for the meteorites. The experimental β_{exp} extracted from the space-resolved data corresponds to Ni isotope partitioning following the power law. This β_{exp} for Ni in Canyon Diablo meteorite cannot result from artificial on-column fractionation, as isotope fractionation on the first column fits a first order mass-dependent fractionation law for isotope partitioning at equilibrium (see Fig. 4), and second and third columns do not introduce any on-column fractionation.

Conclusions

The chemical properties of Ni challenge its isolation from geological matrices, so that target element concentration, isotope ratio measurement precision attainable, separation factors from interfering elements and artificial on-column fractionation have to be carefully considered. A method for high-precision analysis of mass-dependent natural variations of Ni isotope ratios, suitable for applications in the planetary sciences, has been developed and evaluated. The optimized isolation method involves three chromatographic separation steps and was tested for a variety of silicate and iron matrices, and the columns were calibrated to avoid the effect of artificial on-column fractionation on the final results. The separation

Published on 22 May 2015. Downloaded by Universiteit Gent on 16/06/2015 13:15:23.

factors attained were sufficient to avoid spectral interference to a large extent, while the blanks were negligible compared to the amount of Ni processed. Mathematical correction for the remaining isobaric interferences was found to be one of several critical aspects. The overall precision for mass-dependent results is equivalent to or better than that of other methods reported, including double-spiking techniques, and sufficient to distinguish between the stable isotopic signatures of various geological materials. Because the non mass-dependent effects on the isotopic composition of Ni in iron meteorites are so small (<0.3 pptt (ref. 42)), the current level of analytical resolution does not allow to fully quantify such effects. The method developed was applied to terrestrial and extraterrestrial samples and the results of mass-dependent Ni isotope fractionation for several reference materials are in good agreement with previously reported data. Some perspectives for the use of Ni isotope ratios to trace geo- and cosmochemical processes are presented.

Acknowledgements

This research has been funded by the Interuniversity Attraction Poles Program initiated by the Belgian Science Policy Office. Steven Goderis is a postdoctoral fellow of the Research Foundation – Flanders (FWO). The collection of iron meteorites from east Russia and northern Kazakhstan was kindly donated by Dr F. P. Lesnov (IGM SB RAS).

References

1 D. S. Lauretta, *Elements*, 2011, **7**, 11–16.
2 D. Rumble, E. D. Young, A. Shahar and W. Guo, *Elements*, 2011, **7**, 23–28.
3 S. Weyer, A. Anbar, G. Brey, C. Munker, K. Mezger and A. Woodland, *Earth Planet. Sci. Lett.*, 2005, **240**, 251–264.
4 M. E. Sanborn, Q.-Z. Yin and A. J. Irving, in *Lunar and Planetary Science Conference*, 2014, vol. 45, p. 2032.
5 M. E. Wieser and J. R. De Laeter, *Int. J. Mass Spectrom.*, 2009, **286**, 98–103.
6 F. Moynier, J. Blichert-Toft, P. Telouk, J.-M. Luck and F. Albarède, *Geochim. Cosmochim. Acta*, 2007, **71**, 4365–4379.
7 T. Breton and G. Quitté, *J. Anal. At. Spectrom.*, 2014, **29**, 2284–2293.
8 B. Gueguen, O. Rouxel, E. Ponzevera, A. Bekker and Y. Fouquet, *Geostand. Geoanal. Res.*, 2013, **37**, 297–317.
9 E. D. Young, C. E. Manning, E. A. Schauble, A. Shahar, C. A. Macris, C. Lazar and M. Jordan, *Chem. Geol.*, 2015, **395**, 176–195.
10 C. Lazar, E. D. Young and C. E. Manning, *Geochim. Cosmochim. Acta*, 2012, **86**, 276–295.
11 F. Richter, N. Dauphas and F. Teng, *Chem. Geol.*, 2009, **258**, 92–103.
12 G. Ratié, D. Jouvin, J. Garnier, O. Rouxel, S. Miska, E. Guimarães, L. Cruz Vieira, Y. Sivry, I. Zelano, E. Montarges-Pelletier, F. Thil and C. Quantin, *Chem. Geol.*, 2015, **402**, 68–76.
13 N. Estrade, C. Cloquet, G. Echevarria, T. Sterckeman, T. Deng, Y. Tang and J.-L. Morel, *Earth Planet. Sci. Lett.*, 2015, **423**, 24–35.
14 K. O. Konhauser, E. Pecoits, S. V. Lalonde, D. Papineau, E. G. Nisbet, M. E. Barley, N. T. Arndt, K. Zahnle and B. S. Kamber, *Nature*, 2009, **458**, 750–753.
15 S. J. Porter, D. Selby and V. Cameron, *Chem. Geol.*, 2014, **387**, 12–21.
16 L. E. Wasylenki, H. D. Howe, L. J. Spivak-Birndorf and D. L. Bish, *Chem. Geol.*, 2015, **400**, 56–64.
17 V. Cameron and D. Vance, *Geochim. Cosmochim. Acta*, 2014, **128**, 195–211.
18 T.-H.-B. Deng, C. Cloquet, Y.-T. Tang, T. Sterckeman, G. Echevarria, N. Estrade, J.-L. Morel and R.-L. Qiu, *Environ. Sci. Technol.*, 2014, **48**, 11926–119633.
19 V. Cameron, D. Vance, C. Archer and C. H. House, *Proc. Natl. Acad. Sci. U. S. A.*, 2009, **106**, 10944–10948.
20 D. C. Baxter, I. Rodushkin and E. Engström, *J. Anal. At. Spectrom.*, 2012, **27**, 1355–1381.
21 A. Markowski, G. Quitté, A. Halliday and T. Kleine, *Earth Planet. Sci. Lett.*, 2006, **242**, 1–15.
22 A. Scherstén, T. Elliott, C. Hawkesworth, S. Russell and J. Masarik, *Earth Planet. Sci. Lett.*, 2006, **241**, 530–542.
23 R. C. J. Steele, T. Elliott, C. D. Coath and M. Regelous, *Geochim. Cosmochim. Acta*, 2011, **75**, 7906–7925.
24 G. Quitté, M. Meier, C. Latkoczy, A. Halliday and D. Gunther, *Earth Planet. Sci. Lett.*, 2006, **242**, 16–25.
25 K. K. Marhas, S. Amari, F. Gyngard, E. Zinner and R. Gallino, *Astrophys. J.*, 2008, **689**, 622–645.
26 M. Regelous, T. Elliott and C. D. Coath, *Earth Planet. Sci. Lett.*, 2008, **272**, 330–338.
27 D. Malinovsky and F. Vanhaecke, *Anal. Bioanal. Chem.*, 2011, **400**, 1619–1624.
28 V. N. Epov, D. Malinovskiy, F. Vanhaecke, D. Bégué and O. F. X. Donard, *J. Anal. At. Spectrom.*, 2011, **26**, 1142–1156.
29 G. Rugel, T. Faestermann, K. Knie, G. Korschinek, M. Poutivtsev, D. Schumann, N. Kivel, I. Günther-Leopold, R. Weinreich and M. Wohlmuther, *Phys. Rev. Lett.*, 2009, **103**, 072502.
30 S. Tachibana, G. R. Huss, N. T. Kita, G. Shimoda and Y. Morishita, *Astrophys. J.*, 2006, **639**, L87–L90.
31 L. Gall, H. Williams, C. Siebert and A. Halliday, *J. Anal. At. Spectrom.*, 2012, **27**, 137–145.
32 M. Berglund and M. E. Wieser, *Pure Appl. Chem.*, 2011, **83**, 397–410.
33 F. Vanhaecke and L. Moens, *Anal. Bioanal. Chem.*, 2004, **378**, 232–240.
34 W. A. Russell, D. A. Papanastassiou and T. A. Tombrello, *Geochim. Cosmochim. Acta*, 1978, **42**, 1075–1090.
35 D. C. Baxter, I. Rodushkin, E. Engström and D. Malinovsky, *J. Anal. At. Spectrom.*, 2006, **21**, 427–430.
36 J. Woodhead, *J. Anal. At. Spectrom.*, 2002, **17**, 1381–1385.
37 P. Morand and C. J. Allegre, *Earth Planet. Sci. Lett.*, 1983, **63**, 167–176.
38 G. Quitté and F. Oberli, *J. Anal. At. Spectrom.*, 2006, **21**, 1249–1255.
39 F. W. E. Strelow, *Anal. Chem.*, 1960, **32**, 1185–1188.

 This journal is © The Royal Society of Chemistry 2015

Published on 22 May 2015. Downloaded by Universiteit Gent on 16/06/2015 13:15:23.

40 J. Korkisch and S. S. Ahluwalia, *Talanta*, 1967, **14**, 155–170.
41 F. W. E. Strelow, A. H. Victor, C. R. Van Zyl and C. Eloff, *Anal. Chem.*, 1971, **43**, 870–876.
42 D. L. Cook, M. Wadhwa, P. E. Janney, N. Dauphas, R. N. Clayton and A. M. Davis, *Anal. Chem.*, 2006, **78**, 8477–8484.
43 J. H. Chen, D. A. Papanastassiou and G. J. Wasserburg, *Geochim. Cosmochim. Acta*, 2009, **73**, 1461–1471.
44 H. Tang and N. Dauphas, *Earth Planet. Sci. Lett.*, 2012, **359–360**, 248–263.
45 A. Yamakawa, K. Yamashita, A. Makishima and E. Nakamura, *Anal. Chem.*, 2009, **81**, 9787–9794.
46 M. Wahlgren, K. Orlandini and J. Korkisch, *Anal. Chim. Acta*, 1970, **52**, 551–553.
47 A. Victor, *Anal. Chim. Acta*, 1986, **183**, 155–161.
48 F. W. E. Strelow, C. H. S. W. Weinert and C. Eloff, *Anal. Chem.*, 1972, **44**, 2352–2356.
49 F. W. E. Strelow, *Anal. Chim. Acta*, 1990, **233**, 129–134.
50 F. Nelson, R. M. Rush and K. A. Kraus, *J. Am. Chem. Soc.*, 1960, **82**, 339–348.
51 K. A. Kraus, F. Nelson and G. W. Smith, *J. Phys. Chem.*, 1954, **58**, 11–17.
52 E. D. Young, A. Galy and H. Nagahara, *Geochim. Cosmochim. Acta*, 2002, **66**, 1095–1104.
53 F. Wombacher and M. Rehkamper, *J. Anal. At. Spectrom.*, 2003, **18**, 1371–1375.
54 B. Schoene, D. J. Condon, L. Morgan and N. McLean, *Elements*, 2013, **9**, 19–24.
55 J. T. Wasson and G. Kallemeyn, *Geochim. Cosmochim. Acta*, 2002, **66**, 2445–2473.
56 H. Y. J. McSween and G. R. Huss, *Cosmochemistry*, Cambridge University press, 2010.